# Injectionless Full Range Speed Sensorless Control for Synchronous Reluctance Motors based on PWM Current Ripple

Ludovico Ortombina*, Fabio Bernardi†, Luigi Alberti*, and Davide Barater†
*University of Padova, Dept. of Industrial Engineering, Padova, Italy {ludovico.ortombina, luigi.alberti}@unipd.it
†University of Modena and Reggio Emilia, "Enzo Ferrari" Dept. of Engineering, Italy {fabio.bernardi, dbarater}@unimore.it

***Abstract*—This paper deals with a rotor position estimator algorithm for anisotropic motors based on current ripple, and no additional voltage injections are requested. The current trace in the $\alpha\beta$ reference frame is fitted on the implicit ellipse equation by using the least square algorithm, and no parameters are requested for the estimator tuning. A modified modulation scheme is implemented to guarantee a suitable current ripple in all operating conditions. The estimated position is smoothen and adjusted by using a quadrature-PLL, exploiting the obtained sine and cosine components of the rotor position. Simulation results with a synchronous reluctance motor were carried out to prove the effectiveness and the accuracy of the proposed injectionless sensorless algorithm.**

***Index Terms*—ellipse fitting, current ripple, PWM, space vector modulation, sensorless drive, synchronous reluctance motor**

## I. Introduction

Sensorless operation is a modern trend in electric drives, because a cost reduction and an improved system reliability can be achieved. At medium-high speeds, position observers take advantages of a measurable back-electromotive force (BEMF) in order to estimate the rotor position [2], [3]. At low speed and standstill operation, additional voltage signals are commonly injected to excite the system and overcome the low BEMF signal-to-noise ratio. Common methods take advantage of high frequency (HF) voltage injection to retrieve the rotor position [4], [5] but recent solutions exploit low frequency voltage injection to reduce the audible noise [6]. HF injection schemes can be gathered according to the reference frame in which the HF signals are injected, namely, in the stator reference frame (rotating injection) or in the estimated synchronous reference frame (pulsating injection). However, regardless the chosen injection scheme, low speed estimators retrieve the rotor position by exploiting motor magnetic anisotropy which must be detectable [7], [8].

Conventional HF injection schemes modelling and, in turn, observer tuning is not trivial [4]. To simplify the demodulation stage and reduce bandwidth constraints, square wave voltage injection at close to the switching frequency has been proposed [9]. However, their implementation is troublesome in high inductance motors as the amplitude of the injected voltage is a limited resource. To overcome this issue, the inherent current oscillation produced by the pulse-width modulation (PWM) can be used. Indeed, the PWM can be seen as an injected square voltage at the switching frequency $F_\mathrm{s}$ with the largest available voltage superimposed to the reference one. Current ripple has been already exploited by researchers to retrieve the rotor position [10], [11] even if it posed several challenges, due to its fast rate of change and the limited computational power of microprocessors. For example, dedicated Rogowski coils were developed to measure current derivatives in [12] or a modified measurement sequence was developed in [13]. The spread of Field Programmable Gate Array (FPGA) and fast analog-to-digital converter (ADC) pave the way to new control schemes and an easy current oversampling.

In this paper, an estimation algorithm developed for the rotating injection is applied to current ripple [5]. HF currents induced by the rotating injection trace an elliptical trajectory in the $\alpha\beta$ reference frame and it is fitted by means of a least square (LS) algorithm. The rotor position can be retrieved by the ellipse tilt. To apply the same algorithm on the current ripple induced by a chosen PWM modulation without an additional voltage injection, the resemblance between the $\alpha\beta$ current ripple spectra at the switching frequency and the one induced by rotating injection is computed. To guarantee a proper ripple trace in the overall speed range, two different PWM techniques are analysed, namely, the single-edge space vector PWM (SVPWM) and a particular nonzero PWM (NZPWM) one, i.e., the remote state PWM (RSPWM). The induced current by the latter modulation strategy always traces a usable ripple in all operating conditions [14], in particular at low speed where limited modulation indexes are used. Finally, the proposed algorithm is verified on a linear Synchronous Reluctance (SynR) motor since it is characterised by a remarkable anisotropy by means of simulations.

The paper is organised as follow. In Sec. II the motor model and the stator current harmonic analysis is reported. The modulation schemes are described in Sec. III whereas the rotor position estimator as well as the non-zero speed effect compensation algorithm are illustrated in Sec. IV. Finally, simulation results are shown in Sec. V.

This work was supported by the Project "Green SEED: Design of more-electric tractors for a more sustainable agriculture" funded by Italian Ministry for University and Research under PRIN 2017 call, grant n. 2017SW5MRC and by Department of Industrial Engineering, University of Padova, by means of the project SID BIRD211289.

## II. Theoretical Background

### A. Motor equations

The voltage equations of a synchronous reluctance motor in the $dq$ rotating reference frame are:

$$\begin{aligned} u_\mathrm{d} &= R_\mathrm{s} i_\mathrm{d} + L_\mathrm{d}\frac{di_\mathrm{d}}{dt} - \omega_\mathrm{me} L_\mathrm{q} i_\mathrm{q} \\ u_\mathrm{q} &= R_\mathrm{s} i_\mathrm{q} + L_\mathrm{q}\frac{di_\mathrm{q}}{dt} + \omega_\mathrm{me} L_\mathrm{d} i_\mathrm{d} \end{aligned} \tag{1}$$

where $u_\mathrm{d}$ and $u_\mathrm{q}$ are the stator voltages, $i_\mathrm{d}$ and $i_\mathrm{q}$ are the stator currents, $L_\mathrm{d}$ and $L_\mathrm{q}$ are the direct and quadrature inductance, $R_\mathrm{s}$ is the stator resistance and $\omega_\mathrm{me} = p\omega_\mathrm{m}$ are the electrical speed, pole pairs, and mechanical speed, respectively. The motor is considered magnetically linear, namely, motor inductances values is independent from stator currents and cross-differential inductances are neglected. Two auxiliary inductances can be defined as:

$$L_\Sigma \triangleq \frac{L_\mathrm{d} + L_\mathrm{q}}{2} \qquad L_\Delta \triangleq \frac{L_\mathrm{d} - L_\mathrm{q}}{2} \tag{2}$$

where $L_\Sigma$ is the *dq* differential inductance mean value and $L_\Delta$ is the *dq* differential inductance semi-difference value.

### B. Stator currents harmonics analysis

Pulse-width modulation (PWM) is the standard approach adopted to drive the inverter switches in order to obtain the required output voltages. Several PWM schemes have been proposed in literature so far with different features and, the employed ones in this paper are described in Sec. III. Both implemented PWM strategies apply each voltage vector once in a switching period $T_\mathrm{s}$, then their application sequence resembles a rotating injection.

The single phase voltage $u_x$ with respect to the mid-point of the DC bus is equal to $U_\mathrm{dc}/2$ for the period $T_{\mathrm{on},x}$, and equal to $-U_\mathrm{dc}/2$ for the remaining time $T_\mathrm{off}$ of each phase, with $T_{\mathrm{on},x} + T_{\mathrm{off},x} = T_\mathrm{s}$ and $U_\mathrm{dc}$ is the DC link voltage. The output phase voltage can be described by using the Fourier series in complex form and the harmonic component $u_x$ at the switching frequency $F_\mathrm{s} = 1/T_\mathrm{s}$ results as:

$$u_x = \dot{u}_x^+ e^{i\omega_\mathrm{s} t} + \dot{u}_x^- e^{-i\omega_\mathrm{s} t} \qquad \text{with } \dot{u}_x^+ \text{ and } \dot{u}_x^- \in \mathbb{C} \tag{3}$$

where $\omega_\mathrm{s} = 2\pi F_\mathrm{s}$. For the sake of simplicity, the single edge PWM strategy is hereafter analysed but the dissertation can be extended to a generic modulation scheme as well. Starting from the $a$-phase voltage $u_a$, the positive Fourier coefficient $\dot{u}_a^+$ can be computed as:

$$\begin{aligned} \dot{u}_a^+ &= \frac{1}{T_\mathrm{s}}\int_0^{T_\mathrm{s}} u_a(t) e^{-i\omega_\mathrm{s} t} dt \\ &= \frac{1}{T_\mathrm{s}}\left[\int_0^{T_{\mathrm{on},a}} \frac{U_\mathrm{dc}}{2} e^{-i\omega_\mathrm{s} t} dt + \int_{T_{\mathrm{on},a}}^{T_\mathrm{s}} -\frac{U_\mathrm{dc}}{2} e^{-i\omega_\mathrm{s} t} dt\right]. \end{aligned} \tag{4}$$

The signal $u_a$ is real, then the negative coefficient $\dot{u}_a^-$ can be computed as the complex conjugate of the first one. Finally, the desired coefficients results:

$$\dot{u}_a^+ = \frac{iU_\mathrm{dc}}{2\pi}\left[e^{-i\omega_\mathrm{s} T_{\mathrm{on},a}} - 1\right], \quad \dot{u}_a^- = -\frac{iU_\mathrm{dc}}{2\pi}\left[e^{i\omega_\mathrm{s} T_{\mathrm{on},a}} - 1\right]. \tag{5}$$

For a single edge PWM, the $T_{\mathrm{on},a}$ is given by:

$$T_{\mathrm{on},a} = \frac{U_{\alpha\beta}}{U_\mathrm{dc}}\cos(\vartheta_{\alpha\beta}) + \frac{1}{2} \tag{6}$$

where $U_{\alpha\beta}$ and $\vartheta_{\alpha\beta}$ are the magnitude and phase of the voltage vector, respectively. Substituting (5) and (6) in (3) and computing the voltage harmonics of phase $b$ and $c$ in the same way, the Clarke transformation can be applied, so, the $\alpha\beta$ fundamental harmonic voltages $u_{\alpha,c}$ and $u_{\beta,c}$ result:

$$\begin{aligned} u_{\alpha,c} &\approx -\frac{A_1}{2}\left(\cos\left(\omega_\mathrm{s} t + \vartheta_{\alpha\beta}\right) + \cos(-\omega_\mathrm{s} t + \vartheta_{\alpha\beta})\right) \\ u_{\beta,c} &\approx -\frac{A_1}{2}\left(\sin\left(\omega_\mathrm{s} t + \vartheta_{\alpha\beta}\right) + \sin(-\omega_\mathrm{s} t + \vartheta_{\alpha\beta})\right) \end{aligned} \tag{7}$$

where:

$$A_1 = 2\frac{U_\mathrm{dc}}{\pi} J_1\left(\frac{2\pi U_{\alpha\beta}}{U_\mathrm{dc}}\right) \tag{8}$$

and $J_1$ denotes the first order Bessel function and higher order functions, namely, voltage harmonics, are neglected.

The $\alpha\beta$ stator current components at the switching frequency $i_{\alpha,c}$ and $i_{\beta,c}$ due to the approximated first voltage harmonics are:

$$\begin{aligned} i_{\alpha,c} &= -I_\Sigma\left(\frac{\sin(\omega_\mathrm{s} t + \widehat{\vartheta}_\mathrm{me})}{\omega_\mathrm{s} + \widehat{\omega}_\mathrm{me}} + \frac{\sin(\omega_\mathrm{s} t - \widehat{\vartheta}_\mathrm{me})}{\omega_\mathrm{s} - \widehat{\omega}_\mathrm{me}}\right) \\ &\quad - I_\Delta\left(\frac{\sin(\omega_\mathrm{s} t + \widehat{\vartheta}_\mathrm{me} - 2\vartheta_\mathrm{me})}{\omega_\mathrm{s} + \widehat{\omega}_\mathrm{me}} + \frac{\sin(\omega_\mathrm{s} t - \widehat{\vartheta}_\mathrm{me} + 2\vartheta_\mathrm{me})}{\omega_\mathrm{s} + \widehat{\omega}_\mathrm{me}}\right) \\ i_{\beta,c} &= I_\Sigma\left(\frac{\cos(\omega_\mathrm{s} t + \widehat{\vartheta}_\mathrm{me})}{\omega_\mathrm{s} + \widehat{\omega}_\mathrm{me}} - \frac{\cos(\omega_\mathrm{s} t - \widehat{\vartheta}_\mathrm{me})}{\omega_\mathrm{s} - \widehat{\omega}_\mathrm{me}}\right) \\ &\quad - I_\Delta\left(\frac{\cos(\omega_\mathrm{s} t + \widehat{\vartheta}_\mathrm{me} - 2\vartheta_\mathrm{me})}{\omega_\mathrm{s} + \widehat{\omega}_\mathrm{me}} - \frac{\cos(\omega_\mathrm{s} t - \widehat{\vartheta}_\mathrm{me} + 2\vartheta_\mathrm{me})}{\omega_\mathrm{s} - \widehat{\omega}_\mathrm{me}}\right) \end{aligned} \tag{9}$$

where $I_\Sigma = L_\Sigma A_1/(2L_\mathrm{d}L_\mathrm{q})$ and $I_\Delta = L_\Delta A_1/(2L_\mathrm{d}L_\mathrm{q})$, $\widehat{\vartheta}_\mathrm{me}$ and $\widehat{\omega}_\mathrm{me}$ are the estimated electromechanical position and speed, respectively, and $\vartheta_\mathrm{me}$ is the actual electromechanical position. The amplitude of stator current ripple is affected both by the chosen PWM strategy and the voltage reference. It is worth noting that stator current components related to $L_\Delta$ depend on actual rotor position and they can be demodulated with conventional schemes based on modulation/demodulation theory to retrieve the rotor position [15]. Finally, the $L_\Delta$ inductance must be non zero, otherwise rotor position information disappears from (9).

## III. Modulation Schemes

The proposed sensorless algorithm takes advantage of the measured current ripple in order to estimate the rotor position. The effects on the output current ripple of different SVPWM and NZPWM methods, widely analyzed in [16] and [17], are studied and compared. For the sake of clarity, only the PWM techniques whose output current ripple allows the rotor position estimation by means of the ellipse coefficients (the algorithm is detailed in Sec. IV) will be introduced in the following.

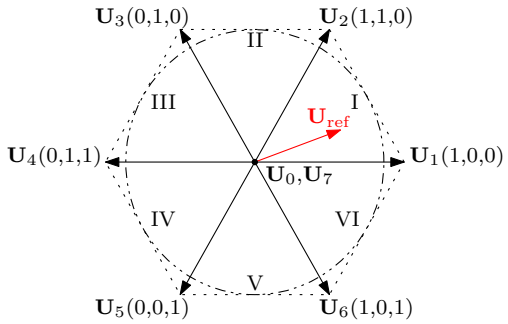


Fig. 1. Space vector diagram for the two-level inverter.

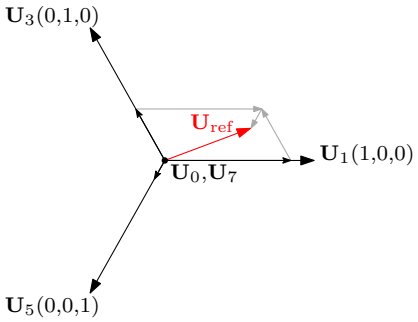


Fig. 2. RSPWM voltage space vectors.

In the conventional SVPWM method, the maximum magnitude of the reference vector $U_{\alpha\beta}^{\max}$ can be represented by the radius of the largest circle inscribed within the hexagon shown in Fig. 1. The hexagon is formed by six active vectors with a length of $2/3U_{\rm dc}$, then $U_{\alpha\beta}^{\max}$ is:

$$U_{\alpha\beta}^{\max} = \frac{2}{3}U_{\rm dc}\frac{\sqrt{3}}{2}. \tag{10}$$

The performance characteristics of a PWM method depend on the modulation index $m_{\rm i}$ [18], that is defined as:

$$m_{\rm i} = \frac{\sqrt{3}U_{\alpha\beta}}{U_{\rm dc}}. \tag{11}$$

and replacing (10) into (11) returns a unitary modulation index $m_{\rm i} = 1$.

The pulse pattern of the conventional symmetrical SVPWM method involves the utilization of both zero-voltage vectors $\mathbf{U}_0$, $\mathbf{U}_7$ during each PWM switching period and it usually chosen since it minimises the current ripple. However, in this work, the current ripple must be detectable, then non conventional PWM strategies are studied. The aim is to implement a modulation able to guarantee a proper detectable ripple in all operating conditions and assures a $m_{\rm i} \in [0,\, 1]$. For these reasons, two different PWM schemes are implemented, one for small modulation index and another for higher one. In both strategies, each voltage vector is applied only once in each switching period.

In the low speed range, namely for small $m_{\rm i}$, the chosen modulation technique is the remote state pulse-width modulation (RSPWM) [19]. It synthesises any feasible voltage vector without using the zero-voltage vectors $\mathbf{U}_0$, $\mathbf{U}_7$, then, the null voltage is obtained by applying all three selected active

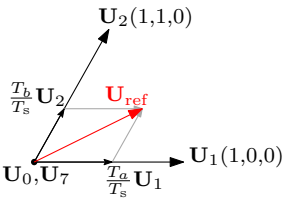


Fig. 3. SVPWM voltage space vectors.

TABLE I
REGION DEPENDENT PULSE PATTERN OF THE IMPLEMENTED PWM METHODS.

| PWM Methods | Sectors | | | | | |
|---|---|---|---|---|---|---|
| | I | II | III | IV | V | VI |
| SVPWM | 7210 | 7230 | 7430 | 7450 | 7650 | 7610 |
| RSPWM | 315 | 315 | 315 | 315 | 315 | 315 |

vector for the same time. The adopted RSPWM switches only between the odd inverter states $\mathbf{U}_1$, $\mathbf{U}_3$, $\mathbf{U}_5$, that are disposed 120° apart from each other as shown in Fig. 2. The operating times of RSPWM (only considering the linear region) are:

$$\begin{cases} T_3 = T_{\rm s}/3 - m_{\rm i}T_{\rm s}\sin\big(\pi/6 - \vartheta_{\alpha\beta}\big)/\sqrt{3} \\ T_5 = T_{\rm s}/3 - m_{\rm i}T_{\rm s}\sin\big(\pi/6 + \vartheta_{\alpha\beta}\big)/\sqrt{3} \\ T_1 = T_{\rm s} - T_3 - T_5 \end{cases} \tag{12}$$

where $T_1$, $T_3$, $T_5$ are the operating time of $\mathbf{U}_1$, $\mathbf{U}_3$, $\mathbf{U}_5$ respectively.

The adopted RSPWM technique utilizes only the vector group $\mathbf{U}_1$, $\mathbf{U}_3$, $\mathbf{U}_5$ and applies the vectors in a fixed sequence throughout the voltage vector space. The dual RSPWM that applies active vectors $\mathbf{U}_2$, $\mathbf{U}_4$, $\mathbf{U}_6$ can be chosen, as well. The main drawback of this switching technique is related to the maximum synthesised voltage $U_{\alpha\beta}^{\max}$ and it can be computed as:

$$U_{\alpha\beta}^{\max} = 0.5 \cdot \frac{2}{3}U_{\rm dc}\frac{\sqrt{3}}{2}. \tag{13}$$

Substituting (13) into (11) return the maximum modulation index when the RSPWM method is adopted, namely, $m_{\rm i} = 1/2$. When $U_{\alpha\beta}^{\max}$ is overcome, the line-to-line voltage and, in turn, the phase current, is distorted.

To overcome the aforementioned constraint, the single edge SVPWM is implemented for higher modulation index. It is akin to the widespread symmetric SVPWM but each voltage vector is applied only once in a switching period and all the three converter legs switch together at the beginning of the switching period. The operating times of SVPWM in the sector I (for $0 \le \vartheta_{\alpha\beta} < \pi/3$) are obtained from the three vectors $\mathbf{U}_1$, $\mathbf{U}_2$, $\mathbf{U}_0$, that are disposed as in Fig. 3, i.e.,

$$\begin{cases} T_1 = m_{\rm i}T_{\rm s}\sin\big(\pi/3 - \vartheta_{\alpha\beta}\big) \\ T_2 = m_{\rm i}T_{\rm s}\sin\vartheta_{\alpha\beta} \\ T_0 = T_{\rm s} - T_1 - T_2 \end{cases} \tag{14}$$

where $T_1, T_2, T_0$ are the operating time of $\mathbf{U}_1$, $\mathbf{U}_2$, null vector, respectively.

The utilized voltage vectors and their sequences applied in the different sectors are given in Tab. I.

## IV. Ellipse Fitting

Conventional low-speed sensorless schemes excite the system by injecting high frequency (HF) voltage signals [4], [20]. Then, induced HF currents are demodulated to retrieve the rotor position. When rotating signal injection is implemented, a different estimation approach was proposed in [5] where the HF currents trace is fitted in time domain to obtained the rotor position. It exploits the elliptical HF current trace in the $\alpha\beta$ plane and that the ellipse tilt is related to the desired position.

In Sec. II-B, the harmonic content of the stator current ripple is analysed and it is similar to the induced one by the rotating injection. In Sec. III, two different PWM strategies that maximise the current ripple are described. In this paper, the ellipse fitting technique is rearranged and applied to the current ripple to estimate the rotor position by exploiting the fact that current ripple spectra is akin to that of induced HF currents by voltage injection. In order to apply the ellipse fitting algorithm [5] on current ripple, it must be revised and divided in two sequential phases. In the former one, the $\alpha\beta$ current ripple is oversampled and values are stored, then the estimation algorithm is applied. To describe the current ripple with an adequate precision, the oversampling frequency $F_{\mathrm{os}}$ must be $N$ times higher than the switching one, with $N > 100$. Finally, the ellipse algorithm is applied on the $N$ stored samples.

Current ripple shape do not resemble an elliptical trace but, Fourier analysis proved that current harmonic at switching frequency describes an ellipse which tilt depends on the rotor position. Then, the $\alpha\beta$ current ripple is fitted on the implicit ellipse equation, namely,:

$$ai_\alpha^2 + bi_\alpha i_\beta + ci_\beta^2 + di_\alpha + ei_\beta = f \tag{15}$$

where $\mathbf{\Theta} = [a, b, c, d, e, f]^T$ is the coefficients vector of a generic ellipse in the $\alpha\beta$ reference frame. The first three coefficients are exclusively dependent on motor inductances and rotor position, indeed, it can be obtained as:

$$\vartheta_{\mathrm{me}} = \frac{1}{2}\mathrm{atan}\frac{b}{a-b}. \tag{16}$$

Moreover, the cosine and sine components of the rotor position can be gotten as:

$$\cos(2\vartheta_{\mathrm{me}}) = \frac{a-c}{\sqrt{b^2+(a-c)^2}} \quad \sin(2\vartheta_{\mathrm{me}}) = \frac{b}{\sqrt{b^2+(a-c)^2}}. \tag{17}$$

The ellipse coefficients $\mathbf{\Theta}$ can be estimated by applying the least square (LS) algorithm on the stored current samples. The $N$ stored current values can be rearranged in the matrix form to describe as many realizations of (15) as:

$$\mathbf{H\Theta} = \mathbf{y} \tag{18}$$

where:

$$\mathbf{H} = \begin{bmatrix} i_{\alpha,1}^2 & i_{\alpha,1}i_{\beta,1} & i_{\beta,1}^2 & i_{\alpha,1} & i_{\beta,1} \\ i_{\alpha,2}^2 & i_{\alpha,2}i_{\beta,2} & i_{\beta,2}^2 & i_{\alpha,2} & i_{\beta,2} \\ \vdots & \vdots & \vdots & \vdots & \vdots \\ i_{\alpha,N}^2 & i_{\alpha,N}i_{\beta,N} & i_{\beta,N}^2 & i_{\alpha,N} & i_{\beta,N} \end{bmatrix}, \quad \mathbf{y} = \begin{bmatrix} f_1 \\ f_2 \\ \vdots \\ f_N \end{bmatrix}. \tag{19}$$

The vector $\mathbf{y}$ is unknown, then (18) can be normalised with respect to $\mathbf{y} = f\mathbf{I}$ which is considered constant and $\mathbf{I}$ is a vector of $N$ ones. The normalised coefficients vector $\mathbf{\Theta}_N = \mathbf{\Theta}/f$ can be estimated as follows:

$$\widehat{\mathbf{\Theta}}_N = \left(\mathbf{H^T H}\right)^{-1}\mathbf{H}^T. \tag{20}$$

Finally, the estimated $\widehat{\mathbf{\Theta}}_N$ coefficients can be used to retrieve the rotor position with (16) or its sine and cosine components with (17) since the normalisation process does not affect the estimated position. It is worth noting that no tuning parameters are required in the estimation process, easing the implementation.

In the stationary reference frame, the current ripple trace in a switching period resemble a triangular with both selected PWM strategies, then only four points are necessary to fully describe it. A tailored current sampling at the switching instants would allow for reducing the stored and analysed samples. However, (18) must be assured overdetermined and with only four samples is not. A solution is to store the midpoint of each segment, which guarantees to reduce the computational burden of the estimation algorithm and the feasibility of (20).

### A. Compensation Algorithm

A snapshot of the proposed rotor position estimation algorithm is depicted in Fig. 4a where the measured $\alpha\beta$ currents are reported as well as the fitted ellipse. On the ellipse center, two segment are drawn which grade is equal to the estimated and the actual electrical rotor position. An estimation error $\widetilde{\vartheta}_{\mathrm{me}} = \vartheta_{\mathrm{me}} - \widehat{\vartheta}_{\mathrm{me}}$ can be observed, due to a non-zero speed distortion effect. Each sample current is characterised by a different rotor position, indeed the motor speed was $\omega_{\mathrm{m}} = 0.1\omega_{\mathrm{N}}$ (p.u.). An estimation error appears by fitting the current ripple without compensating it. To overcome this issue, the compensating algorithm proposed in [5] can be rearranged and the $N$ stored current samples are actualised by assuming the steady-state condition, i.e., a constant speed. The algorithm is:

$$\begin{aligned} i_{\alpha,n}^c &= i_{\alpha,n}\cos\left((n-1)\widehat{\omega}_{\mathrm{me}}T_{\mathrm{s}}\right) - i_{\beta,n}\sin\left((n-1)\widehat{\omega}_{\mathrm{me}}T_{\mathrm{s}}\right) \\ i_{\beta,n}^c &= i_{\alpha,n}\sin\left((n-1)\widehat{\omega}_{\mathrm{me}}T_{\mathrm{s}}\right) + i_{\beta,n}\cos\left((n-1)\widehat{\omega}_{\mathrm{me}}T_{\mathrm{s}}\right) \end{aligned} \tag{21}$$

where the $n$-th sample is forward rotated in the stator reference frame by the electrical angle that the motor swept in $(n-1)T_{\mathrm{s}}$. A smaller index means a newer sampled current and $n \in [0, N-1]$. The current samples $i_{\alpha\beta,n}^c$ are the compensated ones that replace the measured one in the LS matrices (19). Fig. 4b shows the measured (the same as in Fig. 4a) and compensated current and the fitted ellipse on the compensated currents. In this snapshot, the two segments are overlapped, meaning that the non-zero speed effect is fully compensated.

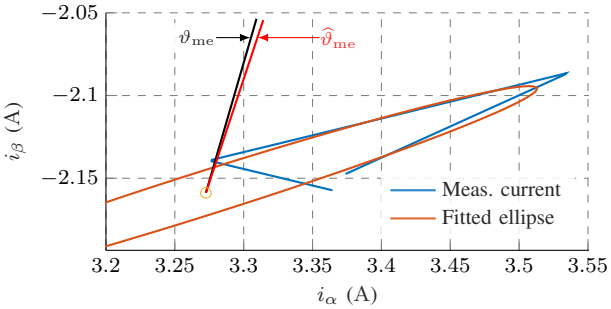


(a) Uncompensated case

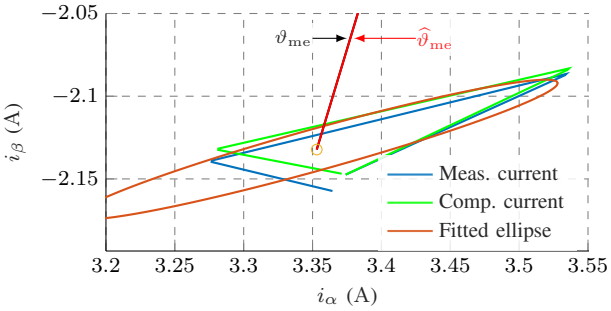


(b) Compensated case

Fig. 4. The non–zero speed effect on the ellipse trajectory and the compensation method result are depicted. The test was carried out at the nominal current and $\omega_{\rm m} = 0.1\omega_{\rm N}$ (p.u.). Measured and compensated currents are shows as well as two segments which tilt is equal to the actual or the estimated position.

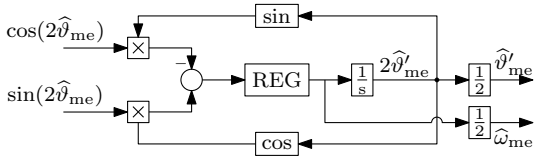


Fig. 5. Quadrature–PLL scheme.

### B. Quadrature PLL

The rotor position can be retrieved by the estimated coefficients $\widehat{\mathbf{\Theta}}_N$ using (16). However, the estimated position only varies in the range $[0, \pi]$ due to the ellipse symmetry over $\pi$ radian. Moreover, the estimated position is noisy since it is obtained by a trigonometric function which argument is a ratio of estimated coefficients and it can become infinite, inducing numerical issues. To get a smoother and reliable rotor position estimation in the proper range, the sine and cosine components of the estimated position computed with (17) feed a quadrature-PLL (Q-PLL) which is reported in Fig. 5. It recovers the rotor position $\widehat{\vartheta}_{\rm me}$ from the trigonometric function and acts as a low-pass filter. Finally, for the sake of simplicity, the PLL output $\widehat{\vartheta}'_{\rm me}$ is indicated only with $\widehat{\vartheta}_{\rm me}$.

## V. Simulation Results

The proposed full range speed sensorless control based on current ripple was verified by means of several simulations, carried out on a linear SynR motor, whose parameters are reported in Tab. II as well as electric drive ones. Fig. 6 shows the whole sensorless electric drive scheme. The number of stored current samples was $N = 7$, namely, the current ripple shape was exploited and the compensation algorithm

TABLE II
Electric motor and drive parameters.

| Parameter | Symbol | Value |
|---|---|---|
| Resistance | $R_{\rm s}$ | $4.8\,\Omega$ |
| Pole pairs | $p$ | 2 |
| $d$-axis inductance | $L_{\rm d}$ | 300 mH |
| $q$-axis inductance | $L_{\rm q}$ | 50 mH |
| Nominal current | $I_{\rm N}$ | 4 A |
| Nominal speed | $\omega_{\rm N}$ | 1500 rpm |
| Switching frequency | $F_{\rm s}$ | 10 kHz |
| DC bus voltage | $U_{\rm dc}$ | 560 V |

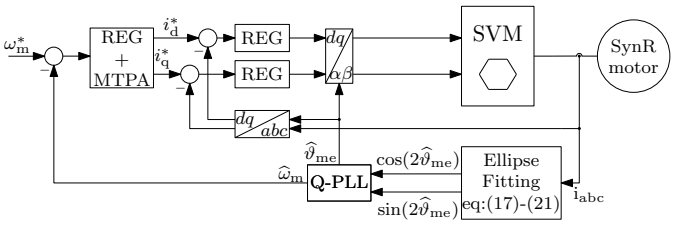


Fig. 6. Proposed sensorless control scheme.

was changed accordingly to a time-varying sampling. All results are expressed in *per unit* (p.u.). and current, torque and speed are normalised with respect to their nominal values. The modulation index threshold between RSPWM operating region and the single edge SVPWM one was set equal to $m_{\rm i} = 0.2$. This choice allows for having a proper and detectable current ripple and maximum available voltage in all operating point.

In order to prove the effectiveness of the proposed algorithm and its dynamic performance, two tests are reported in Fig. 7. The motor under test was speed controlled and both current and speed loops used the estimated quantities. In the first test, the speed reference was ramp-wise varied in 0.3 s from zero to the nominal value whereas the second test was carried out in standstill condition (see Fig. 7a). In both tests, a load torque equal to the nominal one was applied following a 1-s ramp starting at 1.5 s, shown in Fig. 7b. The performance was evaluated by means of the estimation error $\widehat{\vartheta}_{\rm me}$, depicted in Fig. 7c. Finally, the $d$- and $q$-currents are shown in Fig. 7d and Fig. 7e.

The dynamic performance of the electric drive is satisfactory, both at zero speed where the RSPWM was implemented and at high speed with the single-edge SVPWM. Speed and torque references were tracked with a good accuracy, without any undesirable oscillations. Moreover, the nominal (speed and load) point was reached, by the fact that high modulation indexes were achieved by the SVPWM. The position estimation error was always small, even during the fast speed transient. The transition between different modulation scheme was seamless.

## VI. Conclusions

The paper proposes an estimation algorithm that retrieves the rotor position from the current ripple induced by the modulation. First, the current ripple in a switching period is stored and, then, data are fitted on the implicit ellipse equation by means of the least square algorithm, which do not require tuning parameters. To minimise the non-zero speed effect, a tailored algorithm is implemented. The frequency analysis of

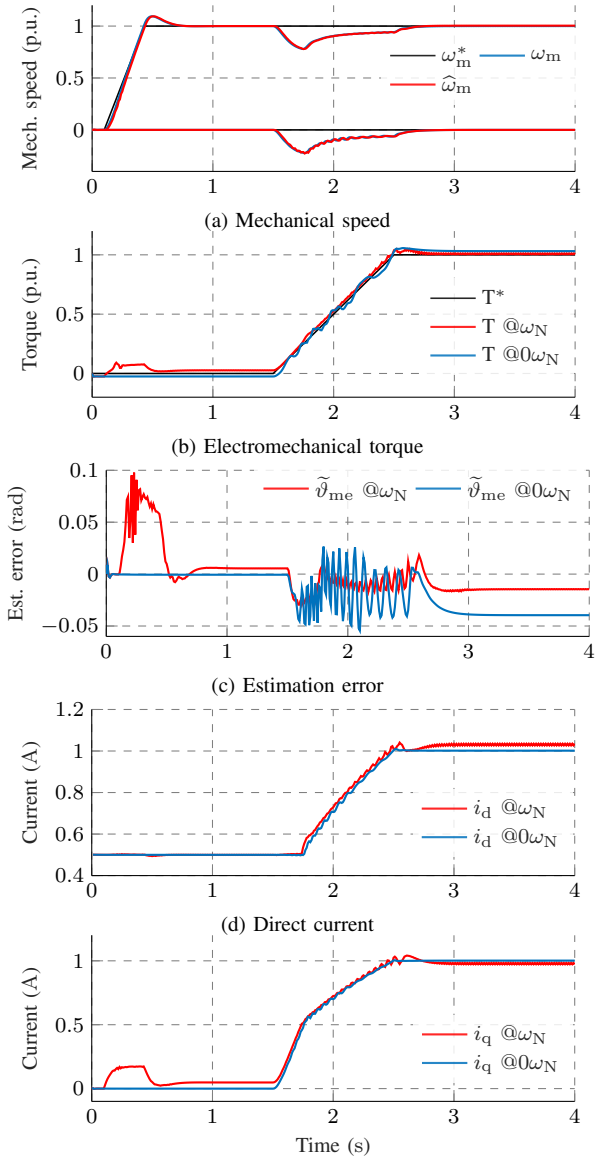


(a) Mechanical speed

(b) Electromechanical torque

(c) Estimation error

(d) Direct current

(e) Quadrature current

Fig. 7. Speed, torque, position estimation error and stator currents of dynamic tests. Two tests at different reference speed (standstill and nominal one) are reported. The nominal torque is applied at t=1.5 s.

the current ripple is reported, proving the equivalence with the conventional rotating injection. Two different PWM strategies are described which have to guarantee a proper ripple from a null to a unitary modulation index. In particular, the RSPWM applies three non-consecutive VSI vector to generate any feasible voltage vector, inducing a suitable ripple even with a null modulation index.

Several simulations were carried out for proving the effectiveness of the proposed algorithm, both at standstill and at the nominal speed with the nominal load. The dynamic performance was noteworthy, with a small estimation error and good tracking capability.

## References


[1] Z. Chen, M. Tomita, S. Doki, and S. Okuma, "An extended electromotive force model for sensorless control of interior permanent-magnet synchronous motors," *IEEE Trans. on Ind. Electron.*, vol. 50, no. 2, pp. 288–295, 2003.

[2] I. Boldea, M. C. Paicu, and G.-D. Andreescu, "Active flux concept for motion-sensorless unified ac drives," *IEEE Trans. on Power Electron.*, vol. 23, no. 5, pp. 2612–2618, 2008.

[3] P. Niedermayr, L. Alberti, S. Bolognani, and R. Abl, "Implementation and experimental validation of ultrahigh-speed pmsm sensorless control by means of extended kalman filter," *IEEE Jour. of Emerg. and Select. Topics in Power Electron.*, vol. 10, no. 3, pp. 3337–3344, 2022.

[4] L. Ortombina, D. Pasqualotto, F. Tinazzi, and M. Zigliotto, "Comprehensive analysis and design of a pulsating signal injection-based position observer for sensorless synchronous motor drives," *IEEE Jour. of Emerg. and Select. Topics in Power Electron.*, vol. 10, pp. 1925–1934, 2022.

[5] L. Ortombina, M. Berto, and L. Alberti, "Sensorless drive for salient synchronous motors based on direct fitting of elliptical-shape high-frequency currents," *IEEE Trans. on Ind. Electron.*, vol. 70, no. 4, pp. 3394–3403, 2023.

[6] R. Brugioni, E. Carfagna, E. Lorenzani, and F. Immovilli, "Critical aspects and strategies for sensorless control of ipmsm based on low-frequency voltage injection," in *2019 IEEE 10th Internat. Symposium on Sensorl. Control for Electr. Drives (SLED)*, 2019, pp. 1–6.

[7] M. Berto, L. Alberti, V. Manzolini, and S. Bolognani, "Computation of self-sensing capabilities of synchronous machines for rotating high frequency voltage injection sensorless control," *IEEE Trans. on Ind. Electron.*, vol. 69, no. 4, pp. 3324–3333, 2022.

[8] G. Galati, L. Ortombina, L. Alberti, and M. Berto, "Investigation on the self-sensing capability of a dual three-phase synchronous reluctance machine," in *2022 Internat. Conf. on Electr. Machines (ICEM)*, 2022, pp. 2256–2262.

[9] Y.-D. Yoon, S.-K. Sul, S. Morimoto, and K. Ide, "High-bandwidth sensorless algorithm for ac machines based on square-wave-type voltage injection," *IEEE Trans. on Ind. Appl.*, vol. 47, pp. 1361–1370, 2011.

[10] M. Giuliato, L. Peretti, F. Tinazzi, and M. Zigliotto, "Sensorless control for a synchronous reluctance motor based on current oversampling using standard pwm excitation," in *The 10th Internat. Conf. on Power Electron., Machines and Drives*, vol. 2020, 2020, pp. 13–18.

[11] A. Varatharajan, P. Pescetto, and G. Pellegrino, "Sensorless synchronous reluctance motor drives: A full-speed scheme using finite-control-set mpc in a projection vector framework," *IEEE Trans. on Ind. Appl.*, vol. 56, no. 4, pp. 3809–3818, 2020.

[12] S. Bolognani, S. Calligaro, R. Petrella, and M. Sterpellone, "Sensorless control for ipmsm using pwm excitation: Analytical developments and implementation issues," in *2011 Symposium on Sensorl. Control for Electr. Drives*, 2011, pp. 64–73.

[13] E. Robeischl and M. Schroedl, "Optimized inform measurement sequence for sensorless pm synchronous motor drives with respect to minimum current distortion," *IEEE Trans. on Ind. Appl.*, vol. 40, no. 2, pp. 591–598, 2004.

[14] M. Hofer, M. Nikowitz, and M. Schroedl, "Sensorless control of a reluctance synchronous machine in the whole speed range without voltage pulse injections," in *2017 IEEE 3rd Internat. Future Energy Electron. Conf. and ECCE Asia*, 2017, pp. 1194–1198.

[15] S. Bolognani, A. Faggion, and L. Sgarbossa, "Rotor position estimation in IPM motor drives based on PWM current harmonics," in *2011 IEEE Inter. Electric Mach. and Drives Conf.*, 2011, pp. 430–435.

[16] A. M. Hava and E. Ün, "Performance analysis of reduced common-mode voltage pwm methods and comparison with standard pwm methods for three-phase voltage-source inverters," *IEEE Trans on Power Electron.*, vol. 24, no. 1, pp. 241–252, 2009.

[17] Zhang, G. Kuang, and L. Long, "Research on reduced common-mode voltage nonzero vector pulse width modulation technique for three-phase inverters," in *Proceedings of The 7th Internat. Power Electron. and Motion Control Conf.*, vol. 4, 2012, pp. 2349–2352.

[18] B. Wu and M. Narimani, *High-power converters and AC drives*. John Wiley & Sons, 2017.

[19] M. Cacciato, A. Consoli, G. Scarcella, and A. Testa, "Reduction of common-mode currents in pwm inverter motor drives," *IEEE Trans. on Ind. Appl.*, vol. 35, no. 2, pp. 469–476, 1999.

[20] D. Raca, P. Garcia, D. D. Reigosa, F. Briz, and R. D. Lorenz, "Carrier-signal selection for sensorless control of pm synchronous machines at zero and very low speeds," *IEEE Trans. on Ind. Appl.*, vol. 46, no. 1, pp. 167–178, 2010.